Measurements of the Ground-State Polarizabilities of Cs, Rb, and K using Atom Interferometry

Maxwell D. Gregoire,[1] Ivan Hromada,[1] William F. Holmgren,[1] Raisa Trubko,[2] and Alexander D. Cronin[1,2]

[1] *Department of Physics, University of Arizona, Tucson, AZ 85721*
[2] *College of Optical Sciences, University of Arizona, Tucson, AZ 85721*

(Dated: July 17, 2015)

We measured the ground-state static electric-dipole polarizabilities of Cs, Rb, and K atoms using a three-nanograting Mach-Zehnder atom beam interferometer. Our measurements provide benchmark tests for atomic structure calculations and thus test the underlying theory used to interpret atomic parity non-conservations experiments. We measured $\alpha_{\rm Cs} = 4\pi\epsilon_0 \times 59.45(11)\mathring{A}^3$, $\alpha_{\rm Rb} = 4\pi\epsilon_0 \times 47.44(9)\mathring{A}^3$, and $\alpha_{\rm K} = 4\pi\epsilon_0 \times 42.97(8)\mathring{A}^3$. We report ratios of polarizabilities $\alpha_{\rm Cs}/\alpha_{\rm Rb} = 1.2532(10)$, $\alpha_{\rm Cs}/\alpha_{\rm K} = 1.3835(9)$, and $\alpha_{\rm Rb}/\alpha_{\rm K} = 1.1040(9)$ with smaller fractional uncertainty because several sources of systematic error are common mode and thus do not affect our measurements of polarizability ratios. Because heavy atoms such as Cs have shorter de Broglie wavelengths and thus small diffraction angles, we developed measurement methods that do not require resolved atom diffraction patterns. Specifically, we used phase choppers to measure atomic beam velocity distributions, and we used electric field gradients to induce atom interference fringe phase shifts proportional to atomic polarizability.

INTRODUCTION

We present absolute and ratio measurements of the static electric-dipole polarizabilities of Cs, Rb, and K made using a Mach-Zehnder three-grating atom interferometer [1, 2] with an electric field gradient interaction region. To our knowledge, this is the first time atom interferometry has been used to measure Cs polarizability. Measuring polarizability by the method described here requires precise measurement of our atom beam's velocity distribution. Because it is challenging to obtain resolved diffraction with a 1500 m/s Cs beam,we did not measure its velocity using diffraction as was done by Ekstrom *et al.* and Holmgren *et al.* [3, 4]. We overcame this obstacle by measuring the beam velocity using phase choppers, invented by Tony Roberts and David Pritchard [5, 6] as a successor to mechanical choppers. Phase choppers, described in Section II, are a pair of electric field gradients chopped on and off at varying frequencies that modify the interference contrast based on the beam velocity distribution. We also improved the configuration of electrodes used to polarize the atoms in our beams so as to reduce systematic errors. This improvement along with the phase choppers allowed us to measure polarizabilities with $< 0.2\%$ uncertainty and polarizability ratios with $< 0.1\%$ uncertainty.

High-precision static-polarizability measurements are used to test atomic structure calculation methods used to calculate polarizabilities, van der Waals coefficients, state lifetimes, branching ratios, and indices of refraction [8]. The quantum many-body theories with relativistic corrections required to describe atoms with many electrons must be highly sophisticated in order to calculate the atomic transition dipole matrix elements accurately in a reasonable amount of computing time [9]. There are many competing atomic structure calculation methods that produce different results. In addition to testing these methods, we can cross-check our results against polarizabilities calculated using recent high-precision measurements of state liftimes. These lifetime-based values have uncertainty comparable to that of our direct polarizability measurements.

Testing Cs atomic structure calculations by measuring $\alpha_{\rm Cs}$ is particularly important for parity non-conservation (PNC) research. The coupling strength of Z^0-mediated interactions between the Cs chiral, valence electron and nuclear neutrons is proportional to $\rho(0)$, the electron density near the nucleus, and the nuclear weak charge Q_W. To calculate Q_W from measurements of coupling strength, PNC researchers must use atomic structure calculations to determine $\rho(0)$ [10, 11]. Our $\alpha_{\rm Cs}$ measurement helps test the methods used to calculated $\rho(0)$.

We were able to report polarizability ratios with $<$ 0.1% uncertainty after considering how several sources of uncertainty, such as the geometry of the electrodes, lead to correlated errors for the different α measurements. We advanced our analysis since Holmgren *et al.* measured polarizability ratios by considering the finite thickness and divergence of the beam, the finite width of the detector, and the effects of de Broglie wavefront curvature induced by our electrodes, as discussed by Hromada *et al.* [12].

Measuring alkali static polarizabilities as a means of testing atomic structure calculations has been of interest to the physics community since 1934 [13], and has been accomplished using deflection [13–15], the E-H gradient balance technique [16, 17], and, most recently, time-of-flight measurements of atoms in a fountain [18] and atom interferometry [3, 4, 19]. In this work, we continue to develop atom interferometry as a technique to precisely measure static polarizabilities.

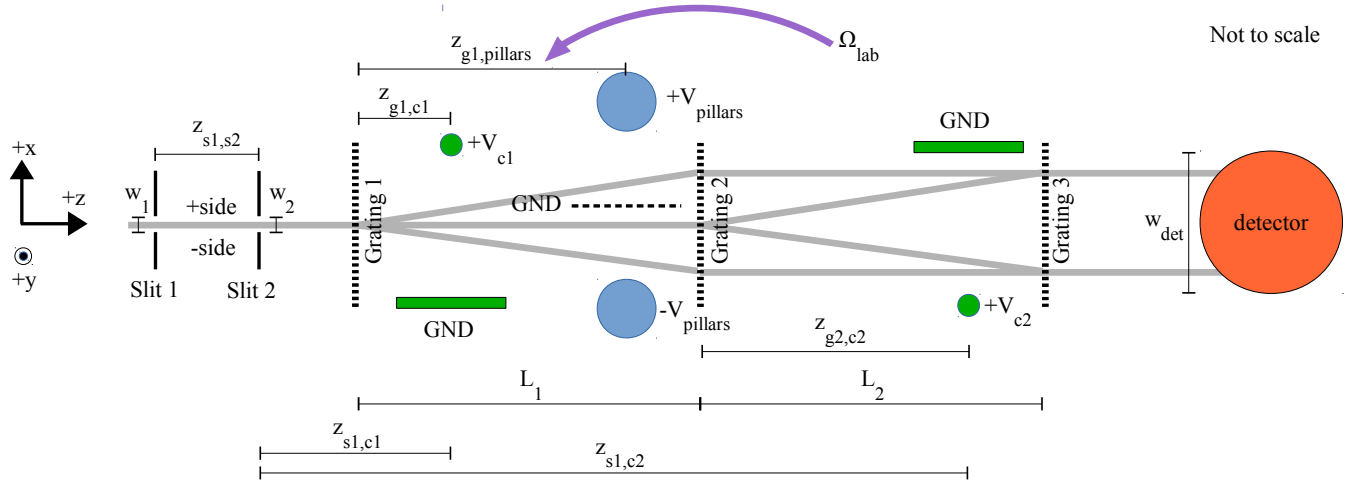

FIG. 1. (Color online) Diagram of the atom interferometry apparatus. The supersonic atom beam is collimated by two slits before entering the three-grating Mach-Zehnder interferometer. Due to the rotation of the Earth, the lab has a rotation rate about the vertical axis of $\Omega_{\mathrm{lab},y} = 38.88\mu$rad/s. The pair of blue circles represents oppositely-charged cylindrical electrodes (extending perpendicular to the page), that form a virtual ground plane between them. These pillars polarize the atoms and thus shift the interference pattern. The phase choppers are represented by the two groups of one green circle and one green rectangle; each phase chopper is a charged wire next to a grounded plane. The geometry terms relevant to the pillars and phase choppers are displayed in Fig. 2 and discussed in the next subsection.

APPARATUS DESCRIPTION AND ERROR ANALYSIS

A schematic diagram of the three-grating Mach-Zehnder atom beam interferometer we use to make our measurements is shown in Fig. 1. We use a thermal, supersonic atom beam [20] seeded with a mixture of 85% He and 15% Ar gas that carries Cs, Rb, and K atoms at approximately 1800 m/s. The atoms pass through two collimating slits and then through three silicon nitride nano-gratings each with period $d_g = 100$ nm. We detect the atoms with a 100 μm-wide platinum wire Langmuir-Taylor detector [21].

The first two gratings form an interference pattern of period d_g at the position of the third grating. By scanning the third grating in the $\pm x$ direction (as defined in Fig. 1), we can cycle between admitting and blocking the interference maxima and thus probe the interference pattern by observing changes in atom flux. In this manner, we observe interference fringes for Cs, Rb, and K using the same collimating slits, gratings, and detector. Changes in x position of the fringes are described by changes in phase Φ according to $\Delta\Phi = 2\pi(\Delta x)/d_g$. The resolution of the fringe pattern is referred to as contrast C and defined in terms of atom flux maxima and minima as

$$C = \frac{(\max) - (\min)}{(\max) + (\min)} \tag{1}$$

For a simple, single-atom interferometer with only two paths, we can shift the phase by adjusting the optical path length difference between those paths. The atom acquires phase by passing through a polarizing electric field $\vec{E}$–the field shifts the atom's energy by $U_{\mathrm{Stark}} = -\frac{1}{2}\alpha\left|\vec{E}\right|^2$, where α is the atom's static polarizability. Since $U_{\mathrm{Stark}} \ll E_{\mathrm{kinetic}}$, we can use the WKB approximation to say

$$\Delta\Phi = \Phi_1 - \Phi_2 = \frac{1}{\hbar v}\int_{\Gamma_1}\frac{\alpha}{2}|\vec{E}|^2 d\Gamma_1 - \frac{1}{\hbar v}\int_{\Gamma_2}\frac{\alpha}{2}|\vec{E}|^2 d\Gamma_2 \tag{2}$$

where Γ_1 and Γ_2 represent the two different paths and v is the atom's velocity. By passing the atoms in the interferometer through a known, non-uniform $\vec{E}$ and measuring v, we can measure α.

The atoms in the beam do not all have the same velocity v and therefore do not all undergo the same $\vec{E}$-induced phase shifts $\Delta\Phi$. Furthermore, the interferometers on the + side and - side of the beamline receive different phase shifts due to gradients in $\vec{E}$. Instead, we consider an ensemble of atoms with first-order diffraction on either side of the beamline with average velocity v_0 and with average phase and contrast defined by the complex value $C_{\mathrm{avg}}e^{i\Phi_{\mathrm{avg}}}$. Without considering this ensemble, we would report α 1.5% too high.

We measure α by polarizing the atoms with a non-uniform electric field created by two oppositely charged pillars parallel with the y axis, indicated in blue in Fig. 1. The field shifts Φ_{avg} by an amount roughly proportional to α/v_0^2. We measure v_0 using phase choppers, which are charged wires parallel with the y axis held near and

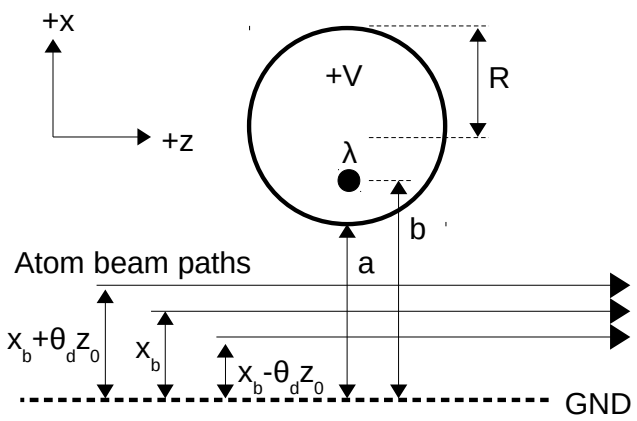

FIG. 2. Diagram showing the dimensions that determine the static electric fields in our interferometer. The circle represents the cross-section of a metal pillar or charged wire with radius R held at voltage V. The GND line represents the ground plane, which may by physical or virtual, a distance a away from the pillar edge. The parameter b is the distance between the ground plane and the effective line charge within the pillar. The atom beam center is a distance x_b away from the ground plane, and the different interferometer arms are separated from their neighbors by a distance $\theta_d z_0$.

parallel to grounded planes, indicated in green in Fig. 1. The phase choppers use the same field geometry as the pillars to apply a $\pm\pi$ phase shift to the atoms. In this section, we will explain how that field geometry induces phase shifts and how we use those fields to measure velocity and, thereby, polarizability.

Phase Shifts with Cylindrical Electrodes

Our methods of measuring both the velocity distribution and polarizability involve applying a phase shift using non-uniform electric fields created by either a cylinder at voltage V next to a grounded plane or two parallel cylinders at $\pm V$ forming an effective ground plane. Both configurations are described by the geometry shown in Fig. 2, and have fields given by

$$\vec{E} = \frac{\lambda}{\pi\epsilon_0}\left[\frac{x-b}{(x-b)^2+z^2} - \frac{x+b}{(x+b)^2+z^2}\right]\hat{x} + \left[\frac{z}{(x-b)^2+z^2} - \frac{z}{(x+b)^2+z^2}\right]\hat{z} \quad (3)$$

The effective line charge density

$$\lambda = 2\pi\epsilon_0 V \ln^{-1}\left(\frac{a+R+b}{a+R-b}\right) \quad (4)$$

exists a distance $b = a\sqrt{1+2R/a}$ away from the ground plane, where a is the distance between the ground plane and the closest cylinder edge, R is the cylinders' radius, and $\hat{x}$ and $\hat{z}$ are shown in Fig. 2.

We use the Residue Theorem to compute the total phase accumulated by an atom traveling through the field along the beamline a distance x_b away from the ground plane. Even though an atom in the beam may be misaligned by an angle of up to 10^{-3} with the different fields' ground planes, we can approximate that atoms always travel parallel to the beamline: the effective path length through the field region grows as $1/\cos\theta \approx 1+\theta^2$, so a misalignment of $\theta = 10^{-3}$ should increase the phase by only one part in 10^6, which is insignificant for our purposes. Therefore, the accumulated phase along the path for a single atom is

$$\Phi(v,x) = \frac{1}{\hbar v}\int_{-\infty}^{\infty}\frac{1}{2}\alpha|\vec{E}|^2 dz = \frac{\lambda^2\alpha}{\pi\epsilon_0^2\hbar v}\left(\frac{b}{b^2-x_b^2}\right) \quad (5)$$

The different paths of the interferometer have different x positions with respect to the electrodes, so the non-uniform electric field causes a differential phase shift. If the center of the field is a distance z_0 downstream of the first grating, for example, the atoms' possible paths are separated by a distance

$$\theta_d z_0 = \frac{\lambda_{dB}}{d_g} z_0 = \frac{h}{mv}\frac{1}{d_g} z_0 \quad (6)$$

where λ_{dB} is the de Broglie wavelength. Paths closer to the effective line charges will acquire more total phase– thus the field causes a differential phase shift. The differential phase shifts for the interferometers on the $j=+1$ and $j=-1$ sides of the beamline (see Fig. 1) are

$$\begin{aligned}\Delta\Phi_{\vec{E},1}(v,x_b) &= \Phi(x_b+\theta_d z_0) - \Phi(x_b)\\ \Delta\Phi_{\vec{E},-1}(v,x_b) &= \Phi(x_b) - \Phi(x_b-\theta_d z_0)\end{aligned} \quad (7)$$

Fig. 3 shows an example of the interference fringes shifting due to an electric-field-induced differential phase shift.

Velocity Measurement

We model the atom beam's velocity distribution as a Gaussian distribution

$$P(v)dv = \frac{r}{v_0\sqrt{2\pi}} e^{-\frac{r^2(v-v_0)^2}{2v_0^2}} \quad (8)$$

where v_0 is the mean velocity and $r = v_0/\sigma_v$ is a measure of the distribution's sharpness. When calculating the average contrast and phase of the ensemble of atoms, we must integrate over this velocity distribution. It is worth noting that the velocity distribution for a super-

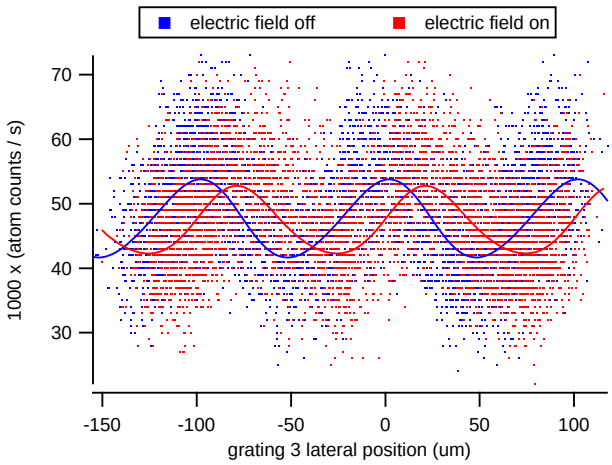

FIG. 3. (Color online) An example of a differential phase shift. The blue and red Cs interference fringes were each observed by moving the third grating in the $\pm x$ direction for 5 seconds. A sine wave was fit to each interference pattern. This figure demonstrates the electric field moving the fringes by about 25 μm, or $d_g/4$, which corresponds to a $\pi/2$ differential phase shift.

sonic atom beam is actually

$$P(v)dv = \frac{1}{\sqrt{2\pi}v_0^4(r^{-1}+3r^{-3})} v^3 e^{-\frac{r^2}{2}\left(\frac{v}{v_0}-1\right)^2} \tag{9}$$

However, both distributions are equally capable of parameterizing the typical velocity distributions of our atom beam. Since v_0 and r are decoupled in the former and not in the latter, we choose to use the former for our data analysis because it simplifies discussion of the results. Using the latter does not change the polarizability result.

To measure v_0 and r, we use phase choppers. Each phase chopper is a charged wire about 1 mm away from a physical ground plane. Chopper 1 is between the first two gratings and chopper 2 is a distance $z_{c1,c2} = (1269.3 \pm 0.25)$ mm downstream of chopper 1, between the last two gratings (see Fig. 1). The voltage on the wire and the distance between the beam and the ground plane are chosen such that chopper 1 shifts the ensemble's average phase by $+\pi$ and chopper 2 shifts the ensemble's average phase by $-\pi$.

When we pulse the choppers on and off at frequency f_c, an atom may receive a net phase shift of $\pm\pi$ or 0 depending on its velocity. Therefore, v_0, r, and f_c determine the fraction of total atoms in the beam which receive a $\pm\pi$ phase shift. This fraction can be quantified by measuring contrast loss C/C_{ref}. To measure v_0 and r, we measure C/C_{ref} vs f_c.

Using phase choppers allows us to measure v_0 and r for Cs without needing to obtain resolved diffraction. In our earlier work, we measured v_0 and r by scanning the detector's x position to observe the diffraction pattern through grating 1. However, since the diffraction angle for Cs is so small, we would need a thinner detector wire and thinner collimating slits to resolve diffraction peaks, which would in turn reduce statistical precision.

We have identified a number of systematic errors in our phase chopper velocity distribution measurements, some of which depend on diffraction angle. These errors must be quantified and reduced in order to measure polarizability ratios between atomic species that typically run with different diffraction angles.

In our previous work [12], we documented the systematic errors that would appear if we were to not accurately know $\Delta L = L_1 - L_2$, where L_1 is the distance between gratings 1 and 2 and L_2 is the distance between gratings 2 and 3. There are two components to this error contribution. The first is that increasing $|\Delta L|$ shifts the interference fringes away from the beamline. We refer to this geometric fringe magnification as the separation phase shift, expressed as

$$\Delta\Phi_{\text{sep},j} = \frac{2\pi}{d_g}\left(\theta_{inc} + \frac{j}{2}\theta_d\right)\Delta L \tag{10}$$

where θ_{inc} is the incident angle of a given atom with de-Broglie wavelength λ_{dB} on grating 1. When the fringes on either side of the beamline shift in opposite directions, they interfere less constructively, which results in contrast loss.

The second component of the error is that, as $|\Delta L|$ increases, the longitudinal region at which the atoms' transverse coherence lengths overlap the most is moved away from grating 3, which also results in contrast loss [22, 23]. Furthermore, the electric fields, such as those created by the phase choppers, act as electrostatic lenses that magnify the interference fringes. This magnification also moves the maximal-overlap region longitudinally. Thus the choppers change the contrast simply by turning on, and changing the longitudinal location of the 3rd grating changes how the choppers modify the contrast. Because the ray optics model that we use to describe our interferometer does not assume finite transverse coherence lengths, we define the longitudinal contrast envelope C_{env}, given by

$$C_{\text{env}}(t) = e^{-\frac{1}{2}\left(\frac{w_1}{L_1 d_g}\right)^2(\Delta L - \Delta L_0(t))^2} \tag{11}$$

where w_1 is the width of the first collimating slit. $\Delta L_0(t)$ is the ΔL for which the measured contrast is maximum given which phase choppers are on as the atoms pass through them.

Uncertainty in ΔL contributes more highly to measurements of atom beams with larger θ_d: the effects described by both $\Delta\Phi_{\text{sep}}$ and $C_{\text{env}}(t)$ are more pronounced when the angles between the paths that converge at grating 3 are greater. Therefore, uncertainty in ΔL is most significant for α_{K} measurements and least significant for α_{Cs}

measurements.

We identified and reduced systematic error by modeling how the collimating slits define the beam's width and divergence and by considering the finite width of the detector, both of which determine how likely it is for atoms of a given velocity to be detected and thus contribute to a measurement of v_0. We accomplish this by integrating over possible trajectories through the slits (in addition to velocity), parameterized by x positions x_1 and x_2 from the centers of slits 1 and 2, in order to calculate the average contrast and phase of the atomic ensemble. We also define $D_j(x_1, x_2, v)$, the probability of an atom with velocity v passing through the slits at positions x_1 and x_2 and diffracting to the j side hitting the detector. This new model also added elements to the error budget: the widths of the collimating slits (w_1 and w_2), the detector width (w_{det}), and the offset of the detector in the x direction (Δx_{det}) determine how likely it is for atoms with certain velocities to be detected.

Uncertainties in w_1, w_2, w_{det}, and Δx_{det} are more significant for beams that are physically wider. In K beams, which have higher θ_d and lower r (i.e. a wider velocity distribution), more of the lower-velocity atoms in the distribution miss the detector. Therefore, uncertainties in the aforementioned quanitities have a higher bearing on how we model the average velocity of detected atoms. However with Cs beams, which have higher average θ_d and r, the detector detects a larger portion of the atoms, rendering the uncertainties in the aforementioned quantities about 10% as significant as with K beams. Completely ignoring this component of the analysis increases systematic error in measured v_0 by 0.05% and r by 10% for a typical K beam, which corresponds to a 0.15% error in α_{K}.

We find that as $|\Delta L|$ increases, the measured v_0 and r become more dependent on the beam width, beam divergence, and detector width. Accordingly, we set $\Delta L = 0$ to reduce contributions to error in reported v_0 from other sources of uncertainty. We begin each day of measurements by setting ΔL to 0, eliminating the need to consider $\Delta\Phi_{\mathrm{sep}}$. We know that if $\Delta\Phi_{\mathrm{sep}}$ were nonzero, we would see the measured phase change as a function of Δx_{det}. We set $\Delta L = 0$ by finding the ΔL for which the measured phase no longer changes as a function of Δx_{det}.

If the interferometer grating bars are significantly nonvertical, it can become necessary to consider the phase shift induced by the component of gravitational acceleration in the plane of the interferometer, which is given by

$$\Delta\Phi_{\mathrm{accel}} = \frac{\pi g \sin(\theta_g)(L_1 + L_2)^2}{2 d_g v^2} \tag{12}$$

where θ_g is the tilt of the grating bars with respect to vertical. However, we eliminated the need to consider $\Delta\Phi_{\mathrm{accel}}$ by rotating our grating bars so that they were sufficiently vertical. We measured θ_g to be $0 \pm 2mrad$. Only if $|\theta_g| >$???? would we need to add $\Delta\Phi_{\mathrm{accel}}$ to our analysis.

Taking all these effects into account, our more complete model for contrast loss as a function of chopping frequency is

$$\begin{aligned}\frac{C}{C_{\mathrm{ref}}}(f_c) = \Bigg| \frac{1}{2} \sum_{j=-1,1} f_c \int_{t=0}^{1/f_c} \int_{x_1=w_1/2}^{w_1/2} \int_{x_2=w_2/2}^{w_2/2} \int_{v=0}^{\infty} \\ P(v) D_j(x_1, x_2, v) C_{\mathrm{env}}(t) \\ \times e^{i\left(\Delta\Phi_{c1,j}(v,x_1,x_2)\Theta\left(t-\frac{1}{2f_c}\right)+\Delta\Phi_{c2,j}(v,x_1,x_2)\Theta\left(t-\frac{z_{c1,c2}}{v}-\frac{1}{2f_c}\right)\right)} \\ \times\, e^{i(\Delta\Phi_{\mathrm{sep},j}(v,x_1,x_2)+\Delta\Phi_{\mathrm{accel}}(v)+\Delta\Phi_{\mathrm{sag}}(v))} dv dx_2 dx_1 dt \Bigg|\end{aligned} \tag{13}$$

where w_1 and w_2 are the widths of collimating slits 1 and 2 and Θ is the Heaviside step function. $\Delta\Phi_{ci,j}(v, x_1, x_2)$ is the differential phase shift induced by chopper i. $\Delta\Phi_{\mathrm{sag}}(v)$ is the Sagnac phase shift, or the phase shift induced by the Earth's rotation [24, 25], and is given by

$$\Delta\Phi_{\mathrm{sag}}(v) = \frac{4\pi L_2^2 \Omega_{\mathrm{lab},y}}{d_g v} \tag{14}$$

The rotation rate of the interferometer about the vertical axis, $\Omega_{\mathrm{lab},y}$, is the product of the Earth's rotation rate and the sine of the lab's latitude. Not including the Sagnac phase shift in the analysis raises reported r by about 1%, which in turn causes α to be reported 0.25% too high.

During times t when the choppers are on, the chopper-induced phase shifts $\Delta\Phi_{ci,j}(v, x_1, x_2)$ are adapted from Eqn. (7) and given by

$$\begin{aligned}\Delta\Phi_{c1,j}(v, x_1, x_2) = \frac{A_{c1}}{v} j \times \\ \left(\frac{1}{b_{c1}^2 - (x_{c1} + \frac{(x_2-x_1)}{z_{s1,s2}} z_{s1,c1} + x_2 + j\theta_d z_{g1,c1})^2} \right. \\ \left. - \frac{1}{b_{c1}^2 - (x_{c1} + \frac{(x_2-x_1)}{z_{s1,s2}} z_{s1,c1} + x_2)^2} \right)\end{aligned}$$

$$\begin{aligned}\Delta\Phi_{c2,j}(v, x_1, x_2) = \frac{A_{c1}}{v} j \times \\ \left(\frac{1}{b_{c2}^2 - (x_{c2} - \frac{(x_2-x_1)}{z_{s1,s2}} z_{s1,c2} - x_2 - j\theta_d z_{g1,g2})^2} \right. \\ \left. - \frac{1}{b_{c2}^2 - (x_{c2} - \frac{(x_2-x_1)}{z_{s1,s2}} z_{s1,c2} - x_2 - j\theta_d z_{g2,c2})^2} \right)\end{aligned} \tag{15}$$

In the above equations, subscripts sn and gn on longitudinal distances z represent collimating slit n and grating

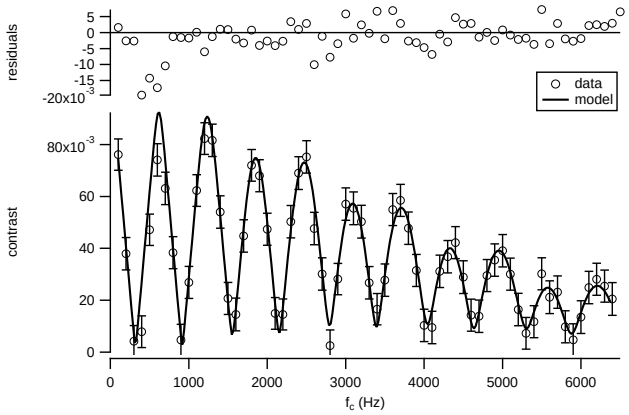

FIG. 4. An example of a measurement of contrast loss vs. phase chopper frequency for a Cs beam. We fit a model to these data that has v_0 and r as fit parameters in order to measure the velocity distribution.

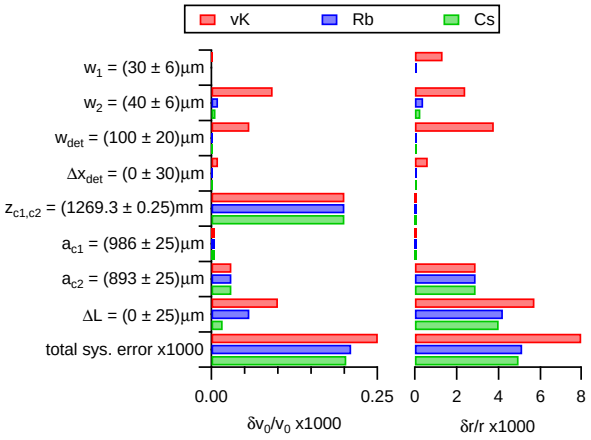

FIG. 5. Systematic error budget for measurements of v_0 and r for our Cs, Rb, and K beams. Parameters w_1, w_2, and w_{det} are the widths of collimating slits 1 and 2 and the detector. a_{ci} is the width of phase chopper i, and $z_{c1,c2}$ is the longitudinal distance between choppers.

n, respectively. A_{c1} and A_{c2} are undetermined constants that represent $\lambda_{ci}^2\alpha/\pi\epsilon_0^2\hbar$ from Eqn. (5).

Instead of requiring accurate knowledge of the chopper voltages and geometries, we measure A_{ci} indirectly. We turn chopper i on and off with a 50 second period to observe the applied phase shift $\Delta\Phi = \Phi_{c1,\mathrm{on}} - \Phi_{\mathrm{ref}}$ and then solve for A_{ci}. When chopper i is off, we observe the reference phase Φ_{ref} and reference contrast C_{ref} given by

$$C_{\mathrm{ref}}e^{\Phi_{\mathrm{ref}}} = C_0 e^{\Phi_0}\frac{1}{2}\sum_{j=-1,1}\int_{v=0}^{\infty}\int_{x_1=w_1/2}^{w_1/2}\int_{x_2=w_2/2}^{w_2/2} P(v)e^{\Delta\Phi_{\mathrm{sag}}(v)+\Delta\Phi_{\mathrm{accel}}(v)+\Delta\Phi_{\mathrm{sep},j}(v)}dv \quad (16)$$

where C_0 is the contrast that would be observed in the absence of $\Delta\Phi_{\mathrm{sag}}(v)$, $\Delta\Phi_{\mathrm{accel}}(v)$, and $\Delta\Phi_{\mathrm{sep}}(v)$, and Φ_0 is an arbitrary phase constant. When chopper i is on, we instead observe

$$C_{ci,\mathrm{on}}e^{\Phi_{ci,\mathrm{on}}} = C_0 e^{\Phi_0}\frac{1}{2}\sum_{j=-1,1}\int_{v=0}^{\infty}\int_{x_1=w_1/2}^{w_1/2}\int_{x_2=w_2/2}^{w_2/2} P(v)e^{\Delta\Phi_{ci,j}(v,x_1,x_2)+\Delta\Phi_{\mathrm{sag}}(v)+\Delta\Phi_{\mathrm{accel}}(v)+\Delta\Phi_{\mathrm{sep},j}(v)}dv \quad (17)$$

Fig. 4 shows an example of a C/C_{ref} vs f_c measurement. For tutorial purposes, Eqns. (13), (16), and (17) include $\Delta\Phi_{\mathrm{sep}}$ and $\Delta\Phi_{\mathrm{accel}}$ even though we have tuned our apparatus so that we need not include them in our analysis.

The error budget for velocity distribution measurement is given in Fig. 5. The measured values of v_0 and r also have statistical error in addition to uncertainty in the fit of measured $C/C_{\mathrm{ref}}(f_c)$ to the model. Uncertainty in the measurement of $\Delta\Phi = \Phi_{c1,\mathrm{on}} - \Phi_{\mathrm{ref}}$ leads to uncertainty in A_{ci}, which in turn propagates forward as additional uncertainty in v_0 and r. The total statistical error in measured v_0 and r is roughly 10× larger than the total systematic error.

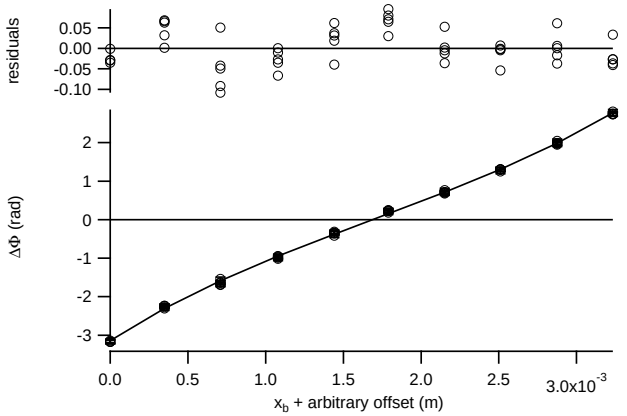

FIG. 6. An example of a measurement of phase shift vs x position of the pillars for a Rb beam. The fit parameters used to fit the model to these data are polarizability and the poles position at which the phase shift is null.

Polarizability Measurement

To measure the atoms' polarizability, we use two parallel, oppositely charged, 1/2-inch-diameter pillars mounted to a single, rigid support structure. The pillars are mounted so that a $(3999.7 \pm 1.0)\mu$m gap exists between them. A motor moves the support structure in the $\pm x$ direction, and a length gauge monitor's the structure's x position. We scan the assembly across the beam so that the beam traverses the gap between the pillars, turning the field on and off as it scans, to observe the phase shift $\Delta\Phi = \Phi_{\mathrm{pillars,on}} - \Phi_{\mathrm{ref}}$ applied by the pillars

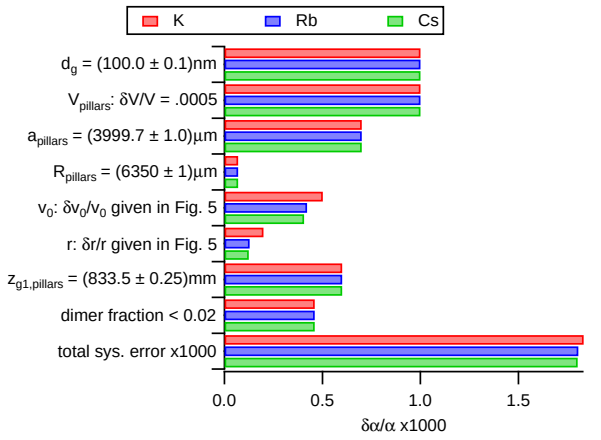

FIG. 7. (Color online) Systematic error budget for polarizability measurements for our Cs, Rb, and K beams. The uncertainties in knowledge of v_0 and r are propagated forward from Fig. 5.

as a function x_b (see an example in Fig. 6). $\Phi_{\rm ref}$ is once again the reference phase and contrast observed when there are no polarizing electric fields present. When the pillars are on, we instead observe

$$C_{\rm pillars,on}e^{\Phi_{\rm pillars,on}} = C_0 e^{\Phi_0}\frac{1}{2}\sum_{j=-1,1}\int_{v=0}^{\infty}P(v) \times e^{\Delta\Phi_{\vec{E},j}(v,x_b)+\Delta\Phi_{\rm sag}(v)+\Delta\Phi_{\rm accel}(v)+\Delta\Phi_{{\rm sep},j}(v)}dv \quad (18)$$

We fit a model to $\Delta\Phi = \Phi_{pillars,\rm on} - \Phi_{\rm ref}$ as shown in Fig. 6, the fit parameters of which are α and the pillars position for which the phase shift is null. Because $\Delta\Phi$ vs pillars position is very linear near the zero crossing, we can determine that zero crossing to very high precision. This changes a previously significant systematic error, associated with measuring the distance between the beam and the physical ground plane, into an insignificant statistical error. Additionally, being able to measure $\Delta\Phi$ on both sides of the virtual ground plane (rather than on only one side of a physical one) makes it unnecessary to consider $\Delta\Phi_{\rm sag}$.

The error budget for the absolute polarizability measurements is shown in Fig. 7. We reduced some error contributions simply by measuring the apparatus geometry more carefully. We constructed the new pillars using steel rods, the widths of which were accurately known to 1μm. This reduced the contribution to $\delta\alpha/\alpha$ from uncertainty in pillars radius by about a factor of 10. We reduced $\delta\alpha/\alpha$ due to uncertainty in the pillars' voltage by a factor of 3 by independently calibrating our voltage supplies. We also reduced $\delta\alpha/\alpha$ due to uncertainty in distance between the pillars and the effective ground plane by sweeping the pillars across the atom beam and observing how far the pillars traveled between points at which the atom beam half-eclipsed each pillar. We were able to measure the distance between the first grating and the pillars to 1/4 mm accuracy rather than 2 mm accuracy.

TABLE I. A typical sequence of measurements during a day of data acquisition. The $+x$ direction is arbitrarily chosen–the important aspect is that we spend an equal amount of time scanning the pillars in each direction so as to minimize possible systematic errors. This sequence of eight measurements is repeated for as long as we choose to acquire data. We end the data acquisition by repeating the first four measurements.

contrast vs chopping freq.
chopper 1 phase
chopper 2 phase
contrast vs chopping freq.
$\Delta\Phi$ vs pillars position ($+x$ direction)
$\Delta\Phi$ vs pillars position ($-x$ direction)
$\Delta\Phi$ vs pillars position ($+x$ direction)
$\Delta\Phi$ vs pillars position ($-x$ direction)

It is important to note that measurements of α are not significantly affected by whether or not we consider $\Delta\Phi_{\rm accel}$ in our polarizability analysis or in our velocity distribution analysis because the grating bars are sufficiently vertical. Also, because we set $\Delta L = 0$, we need not consider $\Delta\Phi_{\rm sep}$. Even if we do consider $\Delta\Phi_{\rm sep}$, we find that our 25μm uncertainty in ΔL does not contribute significantly to uncertainty in measured α. Therefore, $\Delta\Phi_{\rm sag}$, $\Delta\Phi_{\rm accel}$, and $\Delta\Phi_{\rm sep}$ are included in Eqn. (18) for tutorial purposes only–our results are unaffected if we remove them.

Additionally, we found that modeling the beam's thickness and divergence was unnecessary for analysis of polarizability data if $\Delta L = 0$ and becomes increasingly important as $|\Delta L|$ increases. Because we keep ΔL close to 0, we find our reported results do not change if we model the beam's thickness and divergence.

Finally, we report that considering second order diffraction in our model of the interferometer does not change v by more than 0.05 ppt, r by 2 ppt, and α by 0.1 ppt. This is primarily because the fraction of atoms in those interferometer paths is so small. Also, second-order diffraction angles are small enough so that the atoms hit the detector, then they are not sufficiently separated from the first-order interferometer paths.

Data Analysis

A typical sequence of measurements is shown in Table I. We measure the velocity distribution twice between every four scans of the pillars across the beam, and calibrate the phase choppers between each pair of velocity measurements. We interpolate the velocity distribution between measurements to estimate it for each

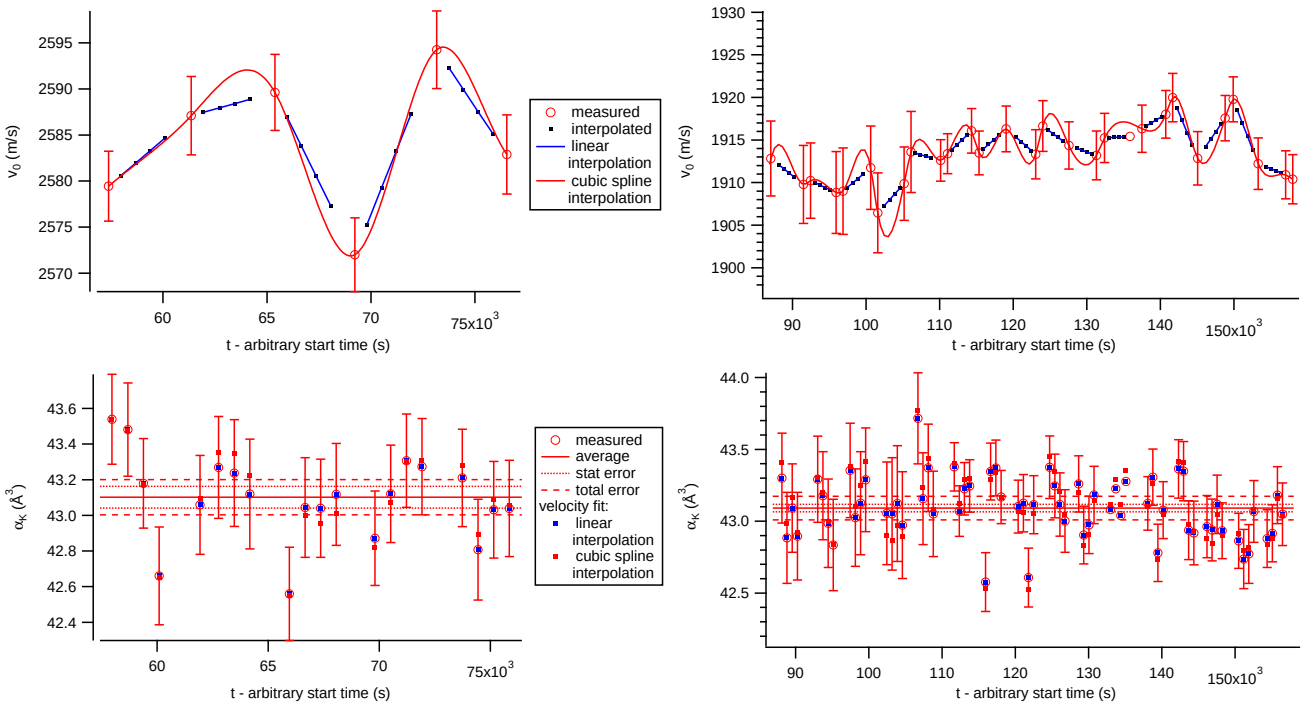

FIG. 8. (Color online) The results of v_0 (top) and α_K (bottom) measurements taken during two different days (left and right). Both linear and cubic spline interpolations between v_0 measurements are reasonable, and higher differences between the two interpolations during α_K measurements increase the error bars on said measurements. For these data, we chose to use linear interpolation because we believe it more accurately represents v_0 vs t–the cubic spline interpolation sometimes gains too much curviture, especially when back-to-back velocity measurements, such as those in the top-left, yield results that differ by an error bar. The red dots on the bottom graphs show what the measured α_K would be if we were to use cubic spline interpolation instead. The top graphs show some typical structures that occur in v_0 vs time. This figure also demonstrates how we obtain the same α_K for very different velocities.

pillars scan. The error bars on each interpolated v_0 and r value are due to the error bars on neighboring measurements and the different ways we believe v_0 and r might be reasonably interpolated. For example, we believe linear and cubic spline interpolations are reasonable, so the error bars at a given time take into account the differences between those interpolations–a larger difference between reasonable interpolations leads to larger error bars on interpolated values. That error is then propagated forward and combined with the statistical error of the fit to $\Delta\Phi$ vs x_b to determine the error bars on the polarizability measurements. Fig. 8 shows an example of interpolations between v_0 measurements at the times of various pillars scans.

RESULTS

Table II shows our absolute measurements of Cs, Rb, and K polarizability and their statistical and systematic errors. The error reported is the standard error of the mean. Table II also shows χ^2/(degree of freedom) for each measurement; we can see that we are operating near the shot-noise limit.

TABLE II. Absolute measurements of Cs, Rb, and K static, ground-state polarizabilities.

Atom	avg v_0 (m/s)	avg r	α(stat.)(sys.) ($\AA^2$)	χ^2/DoF
Cs	1585	19.8	59.45(3)(11)	1.10
Rb	1890	22.9	47.44(3)(9)	1.13
K	2113	13.2	42.97(2)(8)	1.45

Table III shows our ratio measurement results. Even though uncertainties in w_1, w_2, w_{det}, and ΔL contribute differently to uncertainties in measured v_0 and r, the total systematic error for each atom is still effectively the same. Because we used the same apparatus for each absolute measurement, we claim that the systematic errors mentioned in Fig. 5 and Fig. 7 are correlated for different atoms and thus do not contribute to the ratio measurement uncertanties. Thus we are able to achieve $< 0.1\%$ uncertainty in our measured ratios.

TABLE III. Ratio measurements of Cs, Rb, and K static, ground-state polarizabilities.

Atoms	ratio(stat.)
Cs:Rb	1.2532(10)
Cs:K	1.3835(9)
Rb:K	1.1040(9)

TABLE IV. We use the following core polarizabilities ($\alpha_{\rm core}$) and tail polarizabilities ($\alpha_{\rm tail}$) in order to derive polarizabilities from lifetime measurements and matrix elements from polarizabilities. The sources are cited next to each value in the table. We acknowledge that there are several recent theoretical $\alpha_{\rm core}$ values for Cs [38, 55–57], Rb [56, 57], and K [31, 56] that vary by up to 0.03%, 0.07%, and 0.4% of α, respectively.

Atom	$\alpha_{\rm core}(\mathring{A}^3)$	$\alpha_{\rm tail}(\mathring{A}^3)$
Cs	2.34 [58]	0.16 [38]
Rb	1.36 [58]	0.25 [43]
K	0.82 [58]	0.11 [46]

COMPARISONS WITH OTHER WORK

Fig. 9 compares our polarizability measurements with theoretical calculations, semi-empirical calculations, and experimental measurements subsequent to and including Molof *et al.* 's and Hall *et al.* 's 1974 measurements [15, 17]. Our absolute measurements are consistent with all previous absolute measurements. In particular, our $\alpha_{\rm Cs}$ measurement agrees very well with Amini and Gould's recent $\alpha_{\rm Cs}$ measurement [18].

Fig. 9 also compares our ratios to other theoretical, semi-empirical, and experimental ratios. Our ratios are also consistent with all previous ratio measurements except Holmgren *et al.* 's $\alpha_{\rm Rb}/\alpha_{\rm K}$ measurement. We currently do not have an explanation for this discrepancy.

Static polarizabilities can be related to transition dipole matrix elements, state lifetimes, oscillator strengths, and van der Waals coefficients. We will describe those relations and compare our α measurements to α values derived from recent calculations and high-precision measurements of those quantities; those comparisons are shown in Fig. 10. We will also report the values of those quantities that can be derived from our α measurements.

The polarizability (in volume units) of an atom in state i can be written in terms of state lifetimes as

$$\alpha_i = \frac{3c^3}{2}\sum_{k\neq i}\frac{1}{\tau_{ki}\omega_{ik}^4}\frac{g_k}{3g_i} + \alpha_{\rm core} + \alpha_{\rm tail} \qquad (19)$$

where τ_{ki} is the lifetime associated with spontaneous decay from state k to i, ω_{ik} is the transition frequency between states i and k, and $g_n = 2J_n + 1$ is the degeneracy factor for state n. In our case, state i is the ground state. $\alpha_{\rm core}$ is the polarizability of the core electrons, and $\alpha_{\rm tail}$ approximates all the terms not explicitly included in the sum; we only explicitly consider $Ns_{1/2} - Np_{1/2}$ and $Ns_{1/2} - Np_{3/2}$ transitions, and we abbreviate the associated lifetimes to $\tau_{1/2}$ and $\tau_{3/2}$. In our calculations, we use the $\alpha_{\rm core}$ and $\alpha_{\rm tail}$ values indicated in Table IV. The ω_{0k} values are calculated using transition wavelengths reported by NIST [59]. Fig. 10 shows polarizabilities calculated using measurements of $\tau_{1/2}$ and $\tau_{3/2}$ [49–52, 60, 61] and values of $\tau_{1/2,\rm Rb}$ and $\tau_{3/2,\rm Rb}$ inferred in 2002 by Gutterres *et al.* from photo-association data taken in 2000 by Gabbanini *et al.* [62, 63]. Additionally, Rafac and Tanner measured $R_{\rm Cs} = \tau_{1/2,\rm Cs}/\tau_{3/2,\rm Cs} = 1.9809(9)$ in 1998 [64], which we use with Patterson *et al.* 's 2015 measurement of $\tau_{3/2,\rm Cs}$ to report α [54].

We can write α_i in terms of the transition dipole matrix elements as

$$\alpha_i = \frac{e^2}{12\pi\epsilon_0 a_0^4}\sum_{k\neq i}\frac{\left|\langle i|\,\hat{D}\,|k\rangle\right|^2}{\hbar\omega_{ik}} + \alpha_{\rm core} + \alpha_{\rm tail} \qquad (20)$$

where a_0 is the Bohr radius. Again, we only explicitly consider the $Ns_{1/2} - Np_{1/2}$ and $Ns_{1/2} - Np_{3/2}$ matrix elements, which we abbreviate to $D_{1/2}^2$ and $D_{3/2}^2$, respectively. Since $1/\tau_{ik} \propto D_{ik}^2$, we use $R_{\rm Cs}$ along with Porsev *et al.* 's 2010 calculation of $D_{1/2,\rm Cs}^2 = 20.334$ (in atomic units) to report polarizability [64, 65].

In 2002, Derevianko and Porsev derived a method for obtaining values of $D_{1/2,\rm Cs}^2$ from Cs van der Waals C_6 coefficients [38]. Fig. 10 includes α values derived using experimental Cs C_6 measurements in conjunction with Derevianko and Porsev's method and $R_{\rm Cs}$ [38, 64, 66, 67].

Finally, we use our polarizability measurements along with $R_{\rm Cs}$ to report matrix elements $|D|$, lifetimes, and oscillator strengths. α_i is given in terms of oscillator strengths f_{ik} as

$$\alpha_i = \frac{e^2}{4\pi\epsilon_0 m}\sum_{k\neq i}\frac{f_{ik}}{w_{ik}^2} + \alpha_{\rm core} + \alpha_{\rm tail} \qquad (21)$$

where m is the electron mass. Additionally, we use Derevianko and Porsev's method to report a Cs van der Waals C_6 coefficient. These results are displayed in Table V.

As a final comparison, we note that our $\left|D_{1/2,\rm Cs}\right|$ value agrees very well with the theoretical $\left|D_{1/2,\rm Cs}\right|$ calculated by Porsev *et al.* in 2010 for the purpose of interpreting PNC data [65].

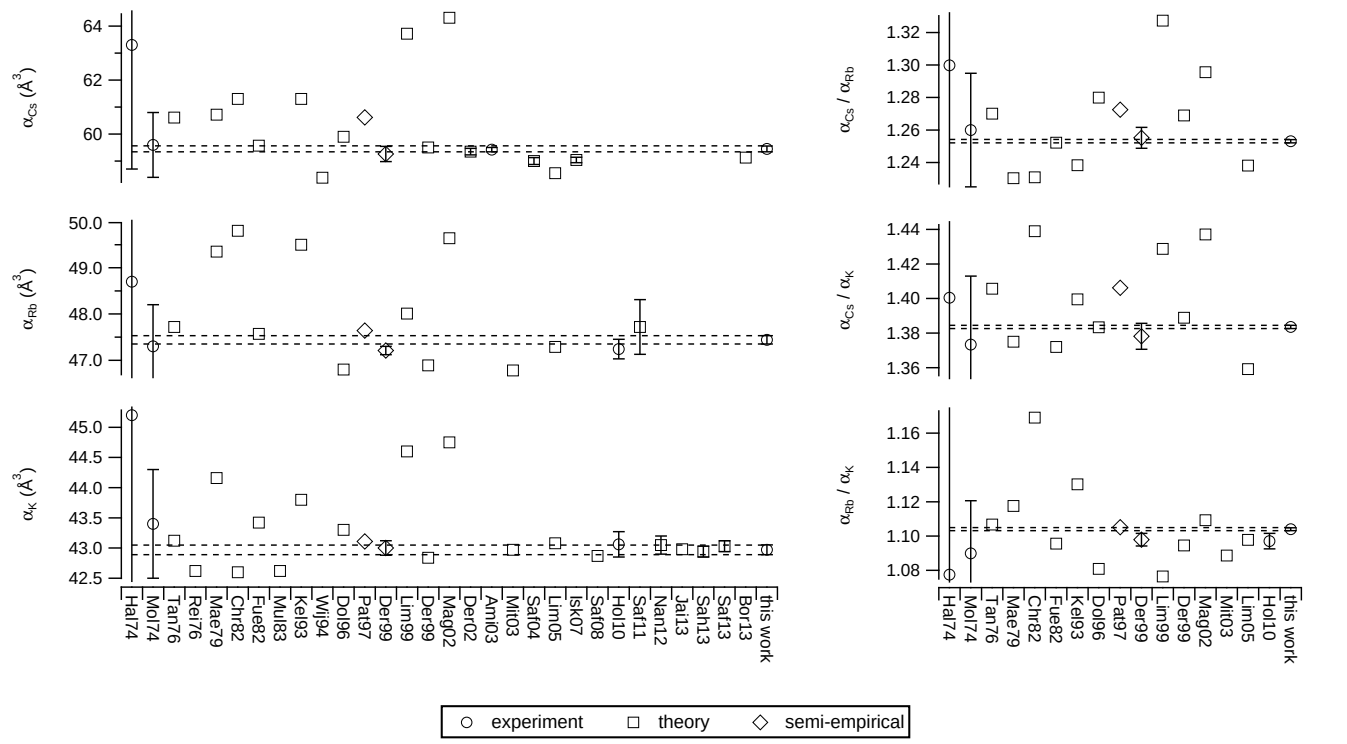

FIG. 9. Our absolute measurements (left) and ratio measurements (right) compared with other measurements, *ab initio* calculations, and semi-empirical calculations [4, 15, 17, 18, 26–48]. The references are represented on the x-axis by the first three letters of the first author's last name followed by the year of publication. Reference Der99 used experimentally-determined electric dipole matrix elements, while reference Pat97 used experimentally-determined energy levels [35, 36]

.

TABLE V. Matrix elements, lifetimes, oscillator strengths, and van der Waals C_6 coefficients calculated from our polarizability measurements along with Rafac and Tanner's R_{Cs} [64]. The C_6 coefficient was calculated using Derevianko and Porsev's method of obtaining C_6 from matrix elements [38]. The matrix elements and C_6 coefficient are expressed in atomic units, while the lifetimes and oscillator strengths are expressed in SI units.

Quantity	Cs	Rb	K
$\lvert D_{1/2}\rvert$	4.515(4)	4.260(4)	4.125(4)
$\lvert D_{3/2}\rvert$	6.354(6)	5.995(6)	5.806(6)
$\tau_{1/2}$ (ns)	34.67(6)	27.44(5)	26.49(5)
$\tau_{3/2}$ (ns)	30.28(6)	26.09(5)	26.40(5)
$f_{1/2}$	0.3461(6)	0.3467(7)	0.3356(6)
$f_{3/2}$	0.3597(7)	0.3498(7)	0.3339(6)
C_6	6905(23)		

OUTLOOK

We are currently exploring ways to measure the polarizability of metastable He, the polarizability of which can be easily calculated. By measuring $\alpha_{\mathrm{Cs}} : \alpha_{\mathrm{He}*}$, we could report an absolute measurement of α_{Cs} with precision comparable to that of the ratios reported here for the benefit of PNC research. Such a measurement would also act as a calibration of the measurements presented in this work, because it would be independent of systematic errors that may affect our absolute measurements.

We are also exploring electron-impact ionization schemes for atom detection, which would allow us to detect a much broader range of atoms and molecules. Our Langmuir-Taylor only allows us to detect alkali metals and some alkaline-Earth metals. Installing a new, "universal" detector would allow us to broaden the scope of atom interferometry as a precision measurement tool.

This work is supported by NSF Grant No. 1306308 and a NIST PMG. M.D.G. and R.T. are grateful for NSF GRFP Grant No. DGE-1143953 for support.

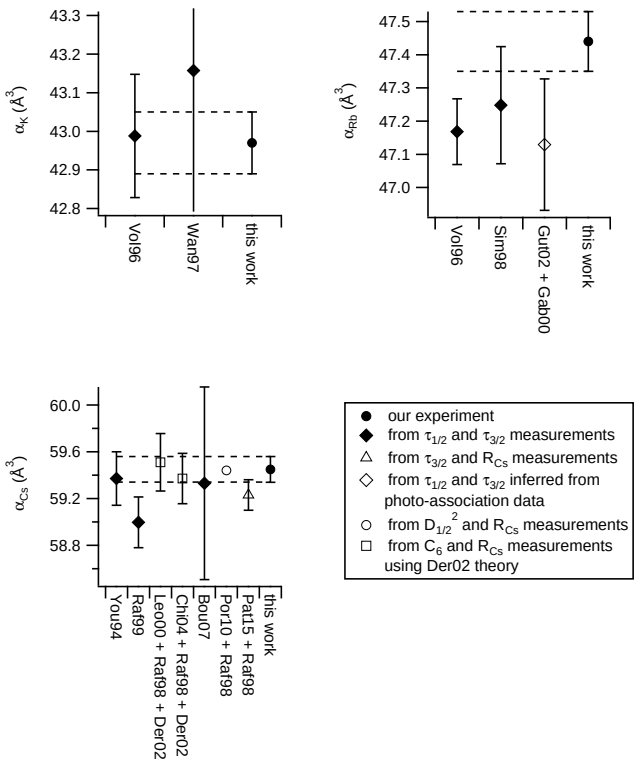

FIG. 10. Comparisons of our measured polarizabilities to polarizabilities derived from measured lifetimes and lifetime ratios, [49–52, 60, 61, 64], lifetimes inferred from photo-association data [62, 63], theoretical D^2 values [65], and van der Waals C_6 measurements [38, 66, 67].

[1] P. Berman, ed., *Atom Interferometry* (Academic Press, San Diego, 1997).

[2] A. D. Cronin, J. Schmiedmayer, and D. E. Pritchard, Reviews of Modern Physics **81**, 1051 (2009), arXiv:0712.3703.

[3] C. R. Ekstrom, J. Schmiedmayer, M. S. Chapman, T. D. Hammond, and D. E. Pritchard, Physical Review A **51**, 3883 (1995).

[4] W. F. Holmgren, M. C. Revelle, V. P. a. Lonij, and A. D. Cronin, Physical Review A - Atomic, Molecular, and Optical Physics **81** (2010), 10.1103/PhysRevA.81.053607, arXiv:1001.3888.

[5] T. D. Roberts, , 188 (2002).

[6] T. D. Roberts, A. D. Cronin, M. V. Tiberg, and D. E. Pritchard, Physical review letters **92**, 060405 (2004).

[7] W. F. Holmgren, I. Hromada, C. E. Klauss, and A. D. Cronin, New Journal of Physics **13** (2011), 10.1088/1367-2630/13/11/115007.

[8] R. C. Hilborn, , 1 (2002).

[9] J. Mitroy, M. S. Safronova, and C. W. Clark, **202001**, 44 (2010), arXiv:1004.3567.

[10] M.-A. Bouchiat and C. Bouchiat, Reports on Progress in Physics **60**, 1351 (1999).

[11] V. a. Dzuba, J. C. Berengut, V. V. Flambaum, and B. Roberts, Physical Review Letters **109**, 1 (2012), arXiv:arXiv:1207.5864v1.

[12] I. Hromada, R. Trubko, W. F. Holmgren, M. D. Gregoire, and A. D. Cronin, Physical Review A **89**, 1 (2014).

[13] H. Scheffers and J. Stark, Physik. Z. **35**, 625 (1934).

[14] G. E. Chamberlain and J. C. Zorn, Physical Review **129**, 677 (1963).

[15] W. D. Hall and J. C. Zorn, Physical Review A **10**, 1141 (1974).

[16] A. Salop, E. Pollack, and B. Bederson, Physical Review **124**, 1431 (1961).

[17] R. W. Molof, The Journal of Chemical Physics **61**, 1816 (1974).

[18] J. M. Amini and H. Gould, Physical review letters **91**, 153001 (2003), arXiv:0305074 [physics].

[19] a. Miffre, M. Jacquey, M. Büchner, G. Trénec, and J. Vigué, European Physical Journal D **38**, 353 (2006), arXiv:0507279 [quant-ph].

[20] G. Scoles, D. Bassi, U. Buck, and D. Lainé, eds., *Atomic and Molecular Beam Methods* (Oxford University Press, New York, Oxford, 1988).

[21] R. Delhuille, a. Miffre, E. Lavallette, M. Büchner, C. Rizzo, G. Trénec, J. Vigué, H. J. Loesch, and J. P. Gauyacq, Review of Scientific Instruments **73**, 2249 (2002), arXiv:0203037 [physics].

[22] C. Champenois, M. Büchner, and J. Vigué, The European Physical Journal D - Atomic, Molecular and Optical Physics **5**, 363 (1999).

[23] B. McMorran and A. D. Cronin, Physical Review A - Atomic, Molecular, and Optical Physics **78**, 1 (2008).

[24] A. Lenef, T. Hammond, E. Smith, M. Chapman, R. Rubenstein, and D. Pritchard, Physical Review Letters **78**, 760 (1997).

[25] M. Jacquey, A. Miffre, G. Trénec, M. Büchner, J. Vigué, and A. Cronin, Physical Review A - Atomic, Molecular, and Optical Physics **78**, 1 (2008), arXiv:0809.0243.

[26] K. T. Tang, The Journal of Chemical Physics **64**, 3063 (1976).

[27] E. A. Reinsch and W. Meyer, Physical Review A **14**, 915 (1976).

[28] W. Kutzelnigg and F. Maeder, Chemical Physics **35**, 397 (1978).

[29] P. A. Christiansen and K. S. Pitzer, Chemical Physics Letters **85**, 4 (1982).

[30] P. Fuentealba, Journal of Physics B: Atomic and Molecular Physics **15**, L555 (1999).

[31] W. Müller, J. Flesch, and W. Meyer, The Journal of Chemical Physics **80**, 3297 (1984).

[32] V. Kello and A. J. Sadlej, Physical Review A **47**, 1715 (1993).

[33] W. a. van Wijngaarden and J. Li, Journal of Quantitative Spectroscopy \& Radiative Transfer **52**, 555 (1994).

[34] M. Dolg, Theoretica Chimica Acta **93**, 141 (1996).

[35] S. H. Patil and K. T. Tang, The Journal of Chemical Physics **106**, 2298 (1997).

[36] a. Derevianko, W. R. Johnson, M. S. Safronova, and J. F. Babb, , 3589 (1998), arXiv:9812028 [physics].

[37] S. Magnier and M. Aubert-Frécon, Journal of Quantitative Spectroscopy and Radiative Transfer **75**, 121 (2002).

[38] A. Derevianko, **65**, 4 (2001), arXiv:0108041 [physics].

[39] J. Mitroy and M. Bromley, Physical Review A **68**, 1 (2003).

[40] M. S. Safronova and C. W. Clark, Physical Review A

- Atomic, Molecular, and Optical Physics **69**, 1 (2004), arXiv:0401060 [physics].
[41] I. S. Lim, P. Schwerdtfeger, B. Metz, and H. Stoll, Journal of Chemical Physics **122** (2005), 10.1063/1.1856451.
[42] U. I. Safronova and M. S. Safronova, , 1 (2008).
[43] M. S. Safronova and U. I. Safronova, Physical Review A - Atomic, Molecular, and Optical Physics **83**, 1 (2011).
[44] D. K. Nandy, Y. Singh, B. P. Shah, and B. K. Sahoo, Physical Review A - Atomic, Molecular, and Optical Physics **86**, 1 (2012), arXiv:1209.5857.
[45] J. Jiang, L. Y. Tang, and J. Mitroy, Physical Review A - Atomic, Molecular, and Optical Physics **87**, 1 (2013), arXiv:1302.6341.
[46] B. K. Sahoo and B. Arora, Physical Review A - Atomic, Molecular, and Optical Physics **87** (2013), 10.1103/PhysRevA.87.023402, arXiv:1212.1814.
[47] M. S. Safronova, U. I. Safronova, and C. W. Clark, Physical Review A - Atomic, Molecular, and Optical Physics **87**, 1 (2013), arXiv:1206.7115.
[48] a. Borschevsky, V. Pershina, E. Eliav, and U. Kaldor, Physical Review A - Atomic, Molecular, and Optical Physics **87** (2013), 10.1103/PhysRevA.87.022502.
[49] L. Young, W. T. Hill, S. J. Sibener, S. D. Price, C. E. Tanner, C. E. Wieman, and S. R. Leone, Physical Review A - Atomic, Molecular, and Optical Physics **50**, 2174 (1994).
[50] U. Volz and H. Schmoranzer, Physica Scripta **T65**, 48 (1996).
[51] H. Wang, J. Li, X. T. Wang, C. J. Williams, P. L. Gould, and W. C. Stwalley, Physical Review A **55**, R1569 (1997).
[52] R. Rafac, C. Tanner, a. Livingston, and H. Berry, Physical Review A **60**, 3648 (1999).
[53] J. F. Sell, B. M. Patterson, T. Ehrenreich, G. Brooke, J. Scoville, and R. J. Knize, Physical Review A **84**, 2 (2011).
[54] B. M. Patterson, J. F. Sell, T. Ehrenreich, M. a. Gearba, G. M. Brooke, J. Scoville, and R. J. Knize, Physical Review A **91**, 1 (2015).
[55] C. J. Sansonetti, K. L. Andrew, and J. Verges, Journal of the Optical Society of America **71**, 423 (1981).
[56] W. Johnson, D. Kolb, and K.-N. Huang, Atomic Data and Nuclear Data Tables **28**, 333 (1983).
[57] M. S. Safronova, W. R. Johnson, and a. Derevianko, **60**, 27 (1999), arXiv:9906044 [physics].
[58] I. S. Lim, J. K. Laerdahl, and P. Schwerdtfeger, Journal of Chemical Physics **116**, 172 (2002).
[59] NIST, "NIST Atomic Spectra Database,".
[60] N. Bouloufa, A. Crubellier, and O. Dulieu, Physical Review A - Atomic, Molecular, and Optical Physics **75**, 1 (2007).
[61] J. Simsarian, L. Orozco, G. Sprouse, and W. Zhao, Physical Review A **57**, 2448 (1998).
[62] C. Gabbanini, a. Fioretti, a. Lucchesini, S. Gozzini, and M. Mazzoni, Physical Review Letters **84**, 2 (2000).
[63] R. Gutterres, C. Amiot, a. Fioretti, C. Gabbanini, M. Mazzoni, and O. Dulieu, Physical Review A **66**, 1 (2002).
[64] R. Rafac and C. Tanner, Physical Review A **58**, 1087 (1998).
[65] S. G. Porsev, K. Beloy, and a. Derevianko, Physical Review D - Particles, Fields, Gravitation and Cosmology **82**, 1 (2010), arXiv:1006.4193.
[66] P. Leo, C. Williams, and P. Julienne, Physical Review Letters **85**, 2721 (2000).
[67] C. Chin, V. Vuletić, A. J. Kerman, S. Chu, E. Tiesinga, P. J. Leo, and C. J. Williams, Physical Review A - Atomic, Molecular, and Optical Physics **70**, 1 (2004).